Available online at www.sciencedirect.com
ScienceDirect
Acta Materialia 58 (2010) 875–885
Acta MATERIALIA
www.elsevier.com/locate/actamat

A ternary phase-field model incorporating commercial CALPHAD software and its application to precipitation in superalloys

Y.H. Wen [a,b,*], J.V. Lill [c], S.L. Chen [d], J.P. Simmons [a]

[a] Air Force Research Laboratory, AFRL/RXLM, Wright-Patterson AFB, OH 45433, USA
[b] UES, Inc., 4401, Dayton-Xenia Road, Dayton, OH 45432, USA
[c] High Performace Technologies, Inc., Wright-Patterson AFB building 676, OH 45433, USA
[d] CompuTherm LLC, 437 S. Yellowstone, Dr. Suite 217, Madison, WI 53719, USA

Received 27 February 2009; received in revised form 1 October 2009; accepted 2 October 2009
Available online 10 November 2009

Abstract

A ternary phase-field model was developed that is linked directly to commercial CALPHAD software to provide quantitative thermodynamic driving forces. A recently available diffusion mobility database for ordered phases is also implemented to give a better description of the diffusion behavior in alloys. Because the targeted application of this model is the study of precipitation in Ni-based superalloys, a Ni–Al–Cr model alloy was constructed. A detailed description of this model is given in the paper. We have considered the misfit effects of the partitioning of the two solute elements. Transformation rules of the dual representation of the $\gamma + \gamma'$ microstructure by CALPHAD and by the phase field are established and the link with commercial CALPHAD software is described. Proof-of-concept tests were performed to evaluate the model and the results demonstrate that the model can qualitatively reproduce observed γ' precipitation behavior. Uphill diffusion of Al is observed in a few diffusion couples, showing the significant influence of Cr on the chemical potential of Al. Possible applications of this model are discussed.

Keywords: Ni–Al–Cr alloys; Ternary phase-field models; Precipitation; Commercial CALPHAD software; Uphill diffusion

1. Introduction

Traditionally, precipitate processes have been studied in a largely empirical fashion, with samples being prepared, carefully heat treated, and characterized. In more recent years, there has been an explosion of materials modeling techniques, the predictive capabilities of which can serve as a guide for experimental efforts to increase the yield above that for simple trial-and-error methods. Therefore, it would be desirable to have an engineering tool that could predict quantitatively the microstructural evolution of an alloy under specified thermodynamic conditions during heat treatment.

The phase-field method has shown great potential for predicting realistic microstructures. However, most phase-field simulations performed to date have been limited to binary systems such as Ni–Al [1–6] and most of the models employed were qualitative. Recently, attempts have been made to develop quantitative phase-field models by specifying the fundamental parameters using thermodynamic and diffusivity databases [7–9,3,4,10,6]. Since Ni-based superalloys contain more than a dozen elements, the development of quantitative multicomponent phase-field models is crucial.

The Ni–Al–Cr system is the most important ternary alloy for Ni-based superalloys, and it provides the basis for simplifying the complex chemistry of more complicated Ni-based superalloys [11]. The importance of this system is reflected by the numerous experimental studies on its phase equilibrium and thermodynamics; for a general review, see Refs. [11,12]. Based upon these extensive experimental studies,

* Corresponding author. Address: Air Force Research Laboratory, AFRL/RXLM, Wright-Patterson AFB, OH 45433, USA. Tel.: +1 937 255 6232; fax: +1 937 656 7292.
E-mail address: youhai.wen@wpafb.af.mil (Y.H. Wen).

1359-6454/$36.00 © 2009 Acta Materialia Inc. Published by Elsevier Ltd. All rights reserved.
doi:10.1016/j.actamat.2009.10.002

critically assessed thermodynamic and kinetic mobility databases are now available in the literature [13,14,11,15].

In this paper we present a ternary phase-field model that links directly to commercial CALPHAD software to obtain the thermodynamic driving forces, and to a recently developed diffusion mobility database [16] that describes the contribution from the disordered face-centered cubic (fcc) phase as well as the ordered $L1_2$ phase. Description of the model is presented in Section 2 followed by the results of some proof-of-concept simulations; a brief discussion of the capability of the model is given in Section 3.

2. The ternary phase-field method

The ternary phase-field model is linked directly to commercial CALPHAD software. We have implemented a diffusion mobility database that became available very recently. This database allows us to have a better description of diffusion behavior near the γ/γ' interfaces and inside the ordered γ' phase. In the phase-field formulation, we have also considered the misfit effect due to the partitioning of the two solute elements.

2.1. Dual representation of the $\gamma + \gamma'$ microstructure by CALPHAD and phase field

There is an incompatibility between the descriptions of ordered domain structure in the CALPHAD and phase-field methods. After reviewing each method, we will develop the transformation rules from one system to the other that is necessary for our link between our phase-field model and the commercial software based on CALPHAD method that we employ.

2.1.1. CALPHAD representation of the $\gamma + \gamma'$ microstructure

In the CALPHAD method, sublattices are used to describe ordering that cannot be described by the regular solution [17]. In the regular solution approximation, all species involved are assumed to be sufficiently similar in terms of size, shape, electronegativity, etc., that random mixing of the solutes is a reasonable approximation. If the species differ significantly, random mixing is not a good approximation and as a consequence the solution cannot be adequately described by the ideal entropy of mixing. In this case, different species may occupy different sublattices (a regular solution is usually assumed within each sublattice) and the distribution of the species are described by their site fractions in the sublattices. Depending on the specific components in a system, the number of sublattices needed for an appropriate description of the system are usually different. For the $\gamma + \gamma'$ microstructure in Ni-based alloys, descriptions using two or four sublattices can be found in the literature [18,19,14].

An example of a binary model using four sublattices to describe the Ni–Al system is given below. Al atoms occupy the corners of the fcc lattice in one of the sublattices while the Ni atoms occupy the center (left side of Fig. 1a). There are three variants (or domains) of this sublattice; one is illustrated on the right side of Fig. 1a where the two Al atoms are on the opposing face centers along the [1 0 0] direction and the Ni atoms occupy the rest of the lattice. The two Al atoms in other two variants similarly occupy opposing face centers but along the [0 1 0] and [0 0 1] directions, respectively. Projections of the distribution of atoms along [0 0 1] direction are illustrated in Fig. 1b for the four different ordered domains.

The site fractions for the sublattices are subject to the normalization condition that summing the fractional occupations over all the sublattices must yield the concentration field:

$$\frac{1}{4}\sum_{s=1}^{4} y^s(\mathbf{r},t) = x(\mathbf{r},t) \tag{1}$$

Following the discussion of the binary system, there are four different domains in terms of each solute elements depending on how they are partitioned in the fcc structure. The site fractions for the ternary alloys are subject to the normalization condition:

$$\frac{1}{4}\sum_{s=1}^{4} y_n^s(\mathbf{r},t) = x_n(\mathbf{r},t) \tag{2}$$

It should be pointed out that the partitioning of the two solute elements must be matched with each other in the precipitate to maintain the $L1_2$ structure. If the sublattices of Cr and Al were different, the Al/Cr ratio would not be the same for all sublattices and an additional ordering reaction would occur resulting from this loss of symmetry. For example, Fig. 2 shows what would happen if one of the base-centered lattice sites was not equivalent to the two face-centered lattice sites with respect to Cr concentration. The difference in Cr concentration in the base-centered site would make this site distinct from the face-centered sites and a tetragonal crystal structure $L1_2$ would result.

2.1.2. Phase-field representation of the $\gamma + \gamma'$ microstructure

In order to describe the binary Ni–Al phase-field model, we require three long-range order (LRO) parameters

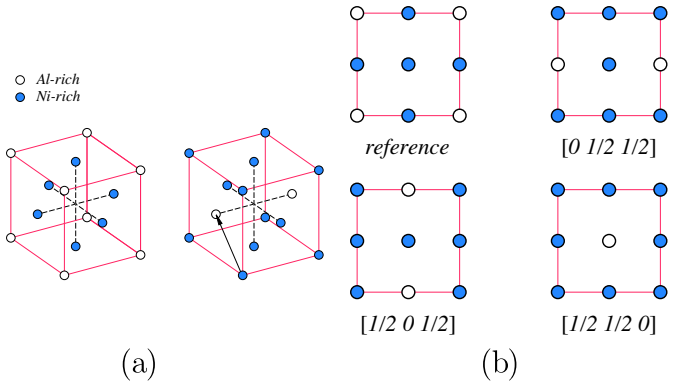

Fig. 1. Illustration of the reference and [0 1/2 1/2] translation domain structure in 3-D (a) and the 2-D projection of the four sublattice structure (b) in the ordered γ' phase.

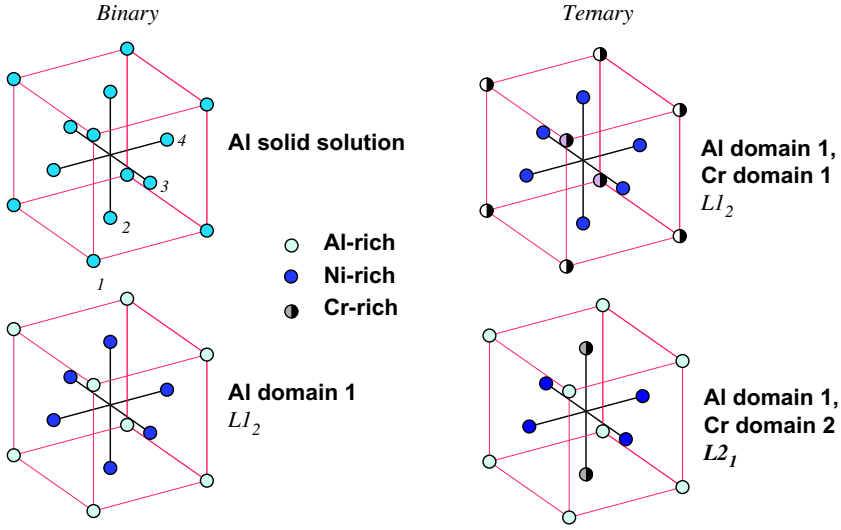

Fig. 2. Four sublattice structures must be matched to maintain the $L1_2$ structure in the ordered γ' phase.

$\eta^p(\mathbf{r},t)$ with $p=1,\ 2,\ 3$ (where $\mathbf{r}$ and t are the spatial coordinates and time) and a concentration field $x(\mathbf{r},t)$. These variables fully describe the partitioning of Al on the four sublattices of the $L1_2$ structure (see Fig. 1) and hence the composition inhomogeneity in the two-phase microstructure $(\gamma+\gamma')$ [1].

Let $\rho(\mathbf{r},t)$ denote the probability of finding solute atom at site $\mathbf{r}$ at time t, the order parameters $\eta^p(\mathbf{r},t)$ are defined as Fourier coefficients in an expansion of the probability $\rho(\mathbf{r},t)$ as in Eq. (3):

$$\rho(\mathbf{r},t)=x(\mathbf{r},t)\{1+\eta^1(\mathbf{r},t)\exp[i\mathbf{k}^1\cdot\mathbf{r}]+\eta^2(\mathbf{r},t)\exp[i\mathbf{k}^2\cdot\mathbf{r}]+\eta^3(\mathbf{r},t)\exp[i\mathbf{k}^3\cdot\mathbf{r}]\} \tag{3}$$

$$\mathbf{k}^1=\frac{2\pi}{a}[1\,0\,0],\mathbf{k}^2=\frac{2\pi}{a}[0\,1\,0],\mathbf{k}^3=\frac{2\pi}{a}[0\,0\,1]$$

The concentration field $x(\mathbf{r},t)$ can then be identified as the probability of finding solute atom at site $\mathbf{r}$ at time t in the completely random alloy, as in Eq. (4):

$$\eta^1(\mathbf{r},t)=\eta^2(\mathbf{r},t)=\eta^3(\mathbf{r},t)=0\Rightarrow\rho(\mathbf{r},t)=x(\mathbf{r},t) \tag{4}$$

Let η° denote the equilibrium LRO parameter at a given composition and temperature. Then four energetically equivalent antiphase domains of the ordered $L1_2$ structure [20] can be defined by specifying the order parameters (η^1,η^2,η^3) as the constant values in Eq. (5):

domain	$\eta^1(\mathbf{r},t)$	$\eta^2(\mathbf{r},t)$	$\eta^3(\mathbf{r},t)$
1	η°	η°	η°
2	$-\eta^\circ$	$-\eta^\circ$	η°
3	$-\eta^\circ$	η°	$-\eta^\circ$
4	η°	$-\eta^\circ$	$-\eta^\circ$

(5)

For example, the first domain is characterized by enriched solute at the eight corners of the cubic cell and depleted solute at the six face centers (Fig. 1a), as in Eq. (6). The other three domains have enriched solute at the two opposing fcc face centers normal to the [0 0 1], [0 1 0], and [1 0 0] directions, respectively, and depleted solute at the other face centers and corners of the cubic cell.

$$\eta^1(\mathbf{r},t)=\eta^2(\mathbf{r},t)=\eta^3(\mathbf{r},t)=\eta^\circ\Rightarrow\rho(\mathbf{r},t)=\begin{cases}x(\mathbf{r},t)[1+3\eta^\circ],\mathbf{k}^1\cdot\mathbf{r}=\mathbf{k}^2\cdot\mathbf{r}=\mathbf{k}^3\cdot\mathbf{r}=2n\pi\\ x(\mathbf{r},t)[1-\eta^\circ],\mathbf{k}^1\cdot\mathbf{r}=\mathbf{k}^2\cdot\mathbf{r}=(2n+1)\pi,\mathbf{k}^3\cdot\mathbf{r}=2n\pi\\ x(\mathbf{r},t)[1-\eta^\circ],\mathbf{k}^2\cdot\mathbf{r}=\mathbf{k}^3\cdot\mathbf{r}=(2n+1)\pi,\mathbf{k}^1\cdot\mathbf{r}=2n\pi\\ x(\mathbf{r},t)[1-\eta^\circ],\mathbf{k}^3\cdot\mathbf{r}=\mathbf{k}^1\cdot\mathbf{r}=(2n+1)\pi,\mathbf{k}^2\cdot\mathbf{r}=2n\pi\end{cases} \tag{6}$$

To extend this binary analysis to the ternary Ni–Al–Cr alloys, an additional set of four field variables are needed to describe the partitioning of Cr in the $L1_2$ structure and the composition inhomogeneity of Cr in the two phases. Consequently, we need a total of eight field variables to describe the microstructure in a ternary phase-field model, i.e. six LRO parameters $\eta_i^p(\mathbf{r},t)$ with $p=1,\ 2,\ 3$ and $i=1,\ 2$; here $i=1$ represents Al and $i=2$ represents Cr. Similarly we need two concentration fields $x_i(\mathbf{r},t)$ to describe the two solutes Al and Cr. The probabilities of finding an Al or Cr solute atom are now extended by analogy for ternary case as in Eq. (7)

$$\rho_n(\mathbf{r},t)=x_n(\mathbf{r},t)\{1+\eta_n^1(\mathbf{r},t)\exp[i\mathbf{k}^1\cdot\mathbf{r}]+\eta_n^2(\mathbf{r},t)\exp[i\mathbf{k}^2\cdot\mathbf{r}]+\eta_n^3(\mathbf{r},t)\exp[i\mathbf{k}^3\cdot\mathbf{r}]\} \tag{7}$$

2.1.3. Transformation of the dual representation between CALPHAD and phase field

In the phase-field representation of the $\gamma+\gamma'$ microstructure in binary systems, we used the variables $\eta^1(\mathbf{r},t),\eta^2(\mathbf{r},t),\eta^3(\mathbf{r},t)$ and $x(\mathbf{r},t)$. In the CALPHAD representation, the free energy is parameterized by the site fractions of the solute, $y^1(\mathbf{r},t),y^2(\mathbf{r},t),y^3(\mathbf{r},t)$ and $y^4(\mathbf{r},t)$. These are completely equivalent formulations that describe ordered alloys. While the order parameters have an explicit meaning for the degree of ordering in the alloy, the site

fractions have a clear correspondence for the occupation of the various sublattices.

We must transform between these equivalent formulations in order to employ the free energies computed with the thermodynamic databases in the phase-field simulations. The correspondence between site fractions of the solute y^s and the phase-field parameters x and η^p is shown in Eq. (8) where each domain y^s represents the site fractions of the solute Al on sublattice s [3].

$$\begin{aligned} y^1(\mathbf{r},t) &= x(\mathbf{r},t)\left[1+\eta^1(\mathbf{r},t)+\eta^2(\mathbf{r},t)+\eta^3(\mathbf{r},t)\right] \\ y^2(\mathbf{r},t) &= x(\mathbf{r},t)\left[1-\eta^1(\mathbf{r},t)-\eta^2(\mathbf{r},t)+\eta^3(\mathbf{r},t)\right] \\ y^3(\mathbf{r},t) &= x(\mathbf{r},t)\left[1-\eta^1(\mathbf{r},t)+\eta^2(\mathbf{r},t)-\eta^3(\mathbf{r},t)\right] \\ y^4(\mathbf{r},t) &= x(\mathbf{r},t)\left[1+\eta^1(\mathbf{r},t)-\eta^2(\mathbf{r},t)-\eta^3(\mathbf{r},t)\right] \end{aligned} \tag{8}$$

Transformation between the dual representations for ternary systems can be obtained by a straightforward extention of Eq. (8):

$$\begin{aligned} y_n^1(\mathbf{r},t) &= x_n(\mathbf{r},t)[1+\eta_n^1(\mathbf{r},t)+\eta_n^2(\mathbf{r},t)+\eta_n^3(\mathbf{r},t)] \\ y_n^2(\mathbf{r},t) &= x_n(\mathbf{r},t)[1-\eta_n^1(\mathbf{r},t)-\eta_n^2(\mathbf{r},t)+\eta_n^3(\mathbf{r},t)] \\ y_n^3(\mathbf{r},t) &= x_n(\mathbf{r},t)[1-\eta_n^1(\mathbf{r},t)+\eta_n^2(\mathbf{r},t)-\eta_n^3(\mathbf{r},t)] \\ y_n^4(\mathbf{r},t) &= x_n(\mathbf{r},t)[1+\eta_n^1(\mathbf{r},t)-\eta_n^2(\mathbf{r},t)-\eta_n^3(\mathbf{r},t)] \end{aligned} \tag{9}$$

2.2. Ternary phase-field evolution equations

The microstructural evolution can be simulated by solving the time-dependent Ginzburg–Landau equation for the six LRO parameters and solving the non-linear Cahn–Hilliard diffusion equation for the two concentration fields:

$$\frac{\partial \eta_i^p}{\partial t} = -L\frac{\delta F}{\delta \eta_i^p} \tag{10}$$

$$\frac{\partial x_i}{\partial t} = V_m^2 \nabla\left[\sum_j M_{ij}\left(\nabla\frac{\delta F}{\delta x_j}\right)\right] \tag{11}$$

Here L is the structural relaxation constant, M_{ij} are the diffusion mobilities, V_m is the molar volume and F is the total free energy of the system.

For the coherent precipitation under consideration, the total free energy consists of the chemical free energy (F_{ch}) and the elastic strain energy (F_{el}):

$$F = F_{ch} + F_{el} \tag{12}$$

According to gradient thermodynamics [21], the chemical free energy should consist of the local chemical free energy and the gradient terms arising from compositional and structural inhomogeneities, i.e.

$$\begin{aligned} F_{ch} = \int_V \Bigg[& f(x_{\mathrm{Al}}, x_{\mathrm{Cr}}, \eta^p_{\mathrm{Al}}, \eta^p_{\mathrm{Cr}}, T) + \frac{1}{2}\sum_{i,j=\mathrm{Al,Cr}}\left(\kappa_{x_{ij}}\nabla x_i \nabla x_j\right) \\ & + \frac{1}{2}\kappa_\eta \sum_{i=\mathrm{Al,Cr}}\sum_p (\nabla \eta_i^p)^2\Bigg] dV \end{aligned} \tag{13}$$

where $f(x_{\mathrm{Al}}, x_{\mathrm{Cr}}, \eta^p_{\mathrm{Al}}, \eta^p_{\mathrm{Cr}}, T)$ is the local chemical free energy that defines the basic thermodynamic properties of the system, $\kappa_{x_{ij}}$ and κ_η are gradient energy coefficients, and it is understood that $p = 1, 2, 3$ for the three components of the LRO parameters. The gradient energy coefficients are used to characterize interfacial energy and interface width [21]. The values of the gradient coefficients are determined by requiring to produce a moderately diffused interface to avoid artifacts in kinetics. The specific values determine the length scale of the simulation through calibration to reproduce the interfacial energy.

2.3. Elastic strain energy

The elastic strain energy arises because of the lattice mismatch between the γ and γ' phases. The misfit strain is assumed to depend only on the compositions, and the linear terms in the expansion of the strain are:

$$\epsilon^\circ_{ij}(\mathbf{r}) = \sum_p \Delta x_p(\mathbf{r})\epsilon^\circ_{ij}(p) \tag{14}$$

$$\Delta x_p(\mathbf{r}) = x_p(\mathbf{r}) - x^\circ_p \tag{15}$$

Here $p = 1$ implies Al and $p = 2$ implies Cr. The quantity Δx_p measures the deviation of the local concentration of a solute from its total site fraction x°_p, and $\epsilon^\circ_{ij}(p)$ is the stress-free transformation strain (SFTS) tensor. For the $\gamma \to \gamma'$ transformation, the SFTS is characterized by a volume change that can be approximated by Vegard's law:

$$\begin{aligned} \epsilon^\circ_{ij}(\mathbf{r}) &= \begin{cases} \epsilon_p & i = j \\ 0 & i \neq j \end{cases} \\ \epsilon_p &= \frac{\partial a(x_{\mathrm{Al}}, x_{\mathrm{Cr}})}{a_\circ \partial x_p} \end{aligned} \tag{16}$$

Here ϵ_p is the concentration coefficient of the crystal lattice parameter, $a(x_{\mathrm{Al}}, x_{\mathrm{Cr}})$ is the lattice parameter of a solid solution with concentration x_{Al} and x_{Cr}, and $a_\circ$ is the lattice parameter of pure solvent. The elastic energy of a two-phase mixture can then be calculated as a function of the concentration profiles:

$$\begin{aligned} F_{el} = & \frac{V}{2}C_{ijkl}\bar{\epsilon}_{ij}\bar{\epsilon}_{kl} - VC_{ijkl}\bar{\epsilon}_{ij}\sum_{p=1}^{2}\epsilon^\circ_{kl}(p)\overline{\Delta x_p} \\ & + \frac{V}{2}C_{ijkl}\sum_{p=1}^{2}\sum_{q=1}^{2}\epsilon^\circ_{ij}(p)\epsilon^\circ_{kl}(q)\overline{\Delta x_p \Delta x_q} \\ & - \frac{1}{2}\sum_{p=1}^{2}\sum_{q=1}^{2}\int' \frac{d^3\mathbf{g}}{(2\pi)^3}B_{pq}(\mathbf{n})\{\Delta x_p\}^*_{\mathbf{g}}\{\Delta x_q\}_{\mathbf{g}} \end{aligned} \tag{17}$$

Here $(\overline{A})$ is the average volume of (A), V is the total volume of the system, C_{ijkl} is the elastic moduli tensor, the notation $\int'$ indicates that the point $n = 0$ is excluded from the integration, and $B_{pq}(\mathbf{n})$ is a two-body interaction potential given by:

$$B_{pq}(\mathbf{n}) = n_i\sigma^\circ_{ij}(p)\Omega_{jk}(\mathbf{n})\sigma_{kl}(q)n_l \tag{18}$$

Here $n = \frac{\mathbf{g}}{|\mathbf{g}|}$ is a unit vector in reciprocal space and n_i is the ith component, $\sigma^\circ_{ij} = C_{ijkl}\epsilon^\circ_{kl}(p)$ and $\Omega_{ij}(\mathbf{n})$ is a Green function tensor which is inverse to the tensor $\Omega^{-1}_{ij}(\mathbf{n}) = C_{ijkl}n_k n_l$,

$\{\Delta x_p\}_{\mathbf{g}}$ is the Fourier transform of Δx_p, and $\{\Delta x_p\}^*_{\mathbf{g}}$ is the complex conjugate of $\{\Delta x_p\}_{\mathbf{g}}$.

2.4. Linking the chemical free energy from thermodynamic databases to phase-field simulations

In the CALPHAD method, the local chemical free energy is expressed as a sum of a reference free energy, an ideal mixing free energy and excess mixing free energy:

$$G(\mathbf{r},T) = G^{ref}(\mathbf{r},T) + G^{id}(\mathbf{r},T) + G^{ex}(\mathbf{r},T) \tag{19}$$

The reference free energy for substitutionally disordered solid solutions is:

$$G^{ref}(\mathbf{r},T) = \sum_{i=1}^{N}\sum_{j=1}^{N}\sum_{k=1}^{N}\sum_{l=1}^{N} y_i^1(\mathbf{r}) y_j^2(\mathbf{r}) y_k^3(\mathbf{r}) y_l^4(\mathbf{r}) G^{\circ}_{ijkl}(T) \tag{20}$$

Here N is the total number of elements in the alloy, and $y_i^s(\mathbf{r})$ is the site fraction of element i on sublattice s with normalizations $\sum_{p=1}^{N} y_p^s(\mathbf{r}) = 1$ and $\frac{1}{4}\sum_{s=1}^{4} y_p^s(\mathbf{r}) = x_p$, i.e. summing the fractional occupancies over all the alloying elements on each sublattice must equal 1, and summing the fractional occupancies over all sublattices for each alloying element must equal the mole fraction of that element. The functions $G^{\circ}_{ijkl}(T)$ are empirically fitted parameters tabulated as functions of temperature in thermodynamic databases. The parameters themselves represent the free energies associated with those phases in which each sublattice is occupied by a single element, the so-called "end-member compounds". These free energies are mixed according to the site fractions to describe a particular alloy. The ideal mixing free energy $G^{id}(\mathbf{r},T)$ is:

$$G^{id}(\mathbf{r},T) = RT\sum_{s=1}^{4} f^s \sum_{n=1}^{N} y_n^s(\mathbf{r}) \ln\left[y_n^s(\mathbf{r})\right] \tag{21}$$

Here R is the gas constant and f^s is the site fraction of sublattice s. This expression gives the entropy of mixing of an ideal solution, enumerating all the equally possible rearrangements of non-interacting atoms within each sublattice. Finally, the excess free energy of mixing $G^{ex}(\mathbf{r},T)$ is:

$$G^{ex}(\mathbf{r},T) = \sum_{s=1}^{4}\sum_{t\neq s}^{4}\sum_{p=1}^{N} y_p^s(\mathbf{r}) \sum_{q=1}^{N} y_q^s(\mathbf{r}) y_p^t(\mathbf{r}) \cdot \sum_{m=1}^{N_{ipq}} \left[y_p^s(\mathbf{r}) - y_q^s(\mathbf{r})\right]^m G^{st}_{pq}(m,T) \tag{22}$$

Here $G^{st}_{pq}(m,T)$ are empirically fitted parameters tabulated as functions of temperature in thermodynamic databases.

The local chemical free energy in Eq. (19) is expressed as a function of the site fractions of the elements on each of the four sublattices. However, in the phase-field description the local chemical free energy is a function of local concentrations and LRO parameters. The two set of parameters are related to each other through Eq. (9).

We have chosen to link our phase-field code to the commercial CALPHAD software Pandat (CompuTherm, LLC). The coupling between the phase-field simulation and the commercial thermodynamic database involves the evaluation of the partial derivatives of the local chemical free energy with respect to the eight site fractions $(y_n^s(\mathbf{r}))$ by Pandat. These partial derivatives are then used to evaluate the partial derivatives of the local chemical free energy with respect to the phase-field parameters, i.e. concentration parameters $(x_n(\mathbf{r}))$ and the LRO parameters $(\eta_n^1(\mathbf{r}), \eta_n^2(\mathbf{r}), \eta_n^3(\mathbf{r}))$, through the chain rules:

$$\frac{\partial f}{\partial x_p} = \sum_{s=1}^{4}\sum_{n=1}^{2} \frac{\partial G}{\partial y_n^s}\frac{\partial y_n^s}{\partial x_p} \quad p = 1,2,3 \tag{23}$$

$$\frac{\partial f}{\partial \eta_p^k} = \sum_{s=1}^{4}\sum_{n=1}^{2} \frac{\partial G}{\partial y_n^s}\frac{\partial y_n^s}{\partial \eta_p^k} \quad k = 1,2,3$$

2.5. Diffusion mobility

The diffusion mobility M_{ij} varies with composition and structure. Due to very limited data on the diffusion mobility from the ordered phase, most simulations to date have used the diffusion mobility of the disordered fcc phase to represent that of the overall behavior of the alloys. In other words, the contribution from the ordered phase is totally ignored although it is well understood that the diffusion behavior and therefore the closely related diffusion mobility in the ordered phase are quite different from that in the disordered fcc phase. Most recently, Campbell has developed a diffusion mobility database that is capable of describing the diffusion mobilities in the γ' phase in the Ni–Al–Cr system [16]. In this work, we adopted this database for the description of the diffusion mobilities in the Ni–Al–Cr system.

The diffusion mobility is expressed as [22]

$$M_{\mathrm{AlAl}} = \frac{1}{V_m} x_{\mathrm{Al}}\left[x_{\mathrm{Cr}}x_{\mathrm{Al}}B_{\mathrm{Cr}} + (1-x_{\mathrm{Al}})^2 B_{\mathrm{Al}} + x_{\mathrm{Al}}x_{\mathrm{Ni}}B_{\mathrm{Ni}}\right] \tag{24}$$

$$M_{\mathrm{AlCr}} = \frac{1}{V_m} x_{\mathrm{Al}}x_{\mathrm{Cr}}\left[-(1-x_{\mathrm{Al}})B_{\mathrm{Al}} - (1-x_{\mathrm{Cr}})B_{\mathrm{Cr}} + x_{\mathrm{Ni}}B_{\mathrm{Ni}}\right]$$

$$M_{\mathrm{CrCr}} = \frac{1}{V_m} x_{\mathrm{Cr}}\left[x_{\mathrm{Al}}x_{\mathrm{Cr}}B_{\mathrm{Al}} + (1-x_{\mathrm{Cr}})^2 B_{\mathrm{Cr}} + x_{\mathrm{Ni}}x_{\mathrm{Cr}}B_{\mathrm{Ni}}\right]$$

where B_i is the atomic mobility of species i. The atomic mobility is usually expressed as:

$$B_i = \frac{1}{RT}\, exp(-\Delta Q_i^*/RT) \tag{25}$$

Here R is the gas constant and Q_i^* is the total activation energy of species i that consists of contributions from the disordered (ΔQ_i^{dis}) and ordered (ΔQ_i^{ord}) states as described below,

$$\Delta Q_i^* = \Delta Q_i^{dis} + \Delta Q_i^{ord} \tag{26}$$

The contribution from the disordered state, ΔQ_i^{dis}, and its composition dependence can be obtained based on

Engstrom and Agren's work [15]. The contribution from the ordered state is described below as in Campbell's work [16],

$$\Delta Q_m^{ord} = \sum_i \sum_{j \neq i} \Delta Q_{i:j}^m \left[y_i^\alpha y_j^\beta - x_i x_j \right] + \sum_i \sum_j \sum_k \Delta Q_{ij:k}^m \left[y_i^\alpha y_j^\alpha y_k^\beta - x_i x_j x_k \right] + \sum_i \sum_j \sum_k \Delta Q_{k:ij}^m \left[y_i^\beta y_j^\beta y_k^\alpha - x_i x_j x_k \right] \quad (27)$$

where the index m, i, j, $k = 1, 2, 3$ represents the three components Al, Cr, Ni in the ternary system. y_i^α is the site fraction of component i on the α sublattice that can be readily converted from the current four-sublattice formulation [19]. $\Delta Q_{i:j}^m$, $\Delta Q_{ij:k}^m$, $\Delta Q_{k:ij}^m$ are the contributions to the activation energy for component m as a result of the chemical ordering of the i, j, and k atoms on the two sublattices. These parameters are well documented in Campbell's work [16].

3. Results and discussion

We have presented a ternary phase-field model that links directly to commercial CALPHAD software and uses a comprehensive diffusion mobility database that describes the contribution from the disordered fcc phase as well as the ordered $L1_2$ phase. Proof of principal simulations were performed to determine if the model can accurately describe the compositional and structural changes associated with the precipitation behavior in $\gamma \rightarrow \gamma'$ phase transformation. The uphill diffusion behavior in Ni–Al–Cr ternary systems is simulated, which is a typical phenomenon of systems with more than two components. In the end of this section, some further opportunities for applying this model are discussed.

As mentioned in Section 2.1.2, the domain structure of the two solute elements must match to maintain the desired $L1_2$ structure in the precipitate. This means that the profiles of three LRO parameters for Al need to overlap with those for Cr. To examine if the model can properly describe precipitation, simulations were run to observe the ordering during the growth of a single precipitate from a small seed in a supersaturated matrix. In these simulations, we assume equilibrium compositions for the seed; also it is fully ordered with $\eta_n^1 = \eta_n^2 = \eta_n^3 = \eta_\circ$, where $n = 1, 2$ represent respectively solute Al and Cr. Two different bulk compositions in the matrix were chosen to investigate the possible effect of varying the concentration partitioning on the ordering. The compositions were Ni–10Al–10Cr at.% and Ni–15Al–5Cr at.%, and the temperature was 873 K.

Fig. 3 shows the growth of the precipitate and the evolution of the concentrations and the LRO parameters η_n^1 for Al($n = 1$) and Cr($n = 2$) in Ni–10Al–10Cr at.%. It was observed that η_n^2 and η_n^3 follow the evolution of η_n^1 very closely. It is clearly show that the two order parameters η_1^1 and η_2^1 follow one another. The compositions in the precipitate show an enrichment in Al and a depletion in Cr as expected from the ternary phase diagram. This demonstrates that the model can adequately describe the compositional and structural changes associated with precipitation.

For alloy Ni–15Al–5Cr at.%, the partitioning of Cr in the two phases γ and γ' is about equal based on the ternary phase diagram. Therefore, the growth of the γ' precipitate is expected to involve mainly diffusion of Al while the diffusion of Cr should be insignificant. This is indeed the case in the results of the simulation as shown in Fig. 4. The Cr composition is largely the same in the two phases except near the interfaces where significant variation is present. However, the lack of Cr partitioning does not affect the ordering behavior at all and the two-order parameters still closely follow each other with the growth of the precipitate. This is a further indication that the model can properly describe the $L1_2$ structural change associated with the precipitation process.

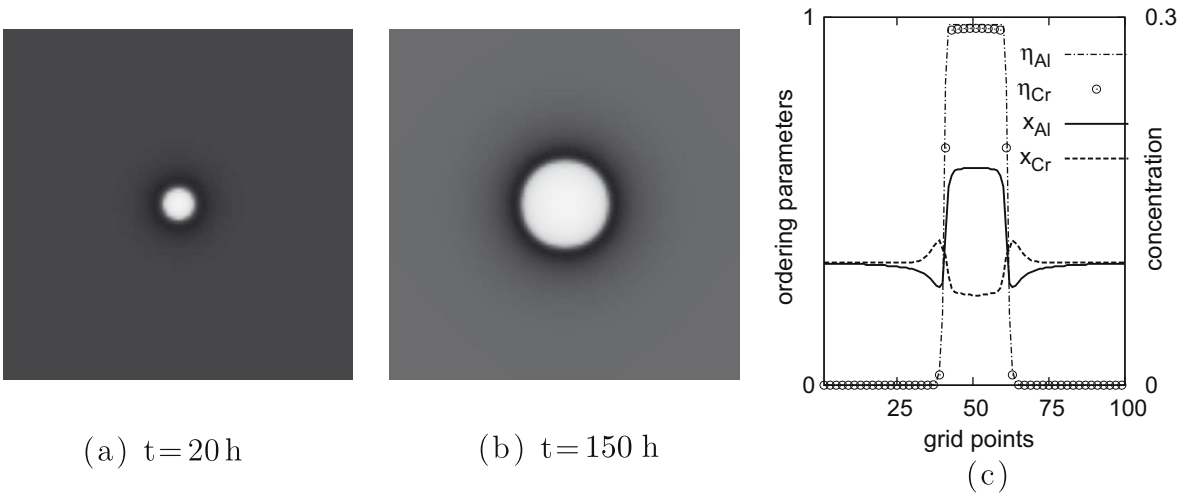

Fig. 3. Growth of the precipitate from a small seed and the accompanying evolution of concentrations and a representative LRO parameter η^1 for Al and Cr in Ni–10Al–10Cr at.% alloy. Note different y-scale is applied in (c) for the ordering and concentration profiles. The equilibrium concentrations of the precipitate are $X_{Al}^{eq} = 0.15$ and $X_{Cr}^{eq} = 0.08$.

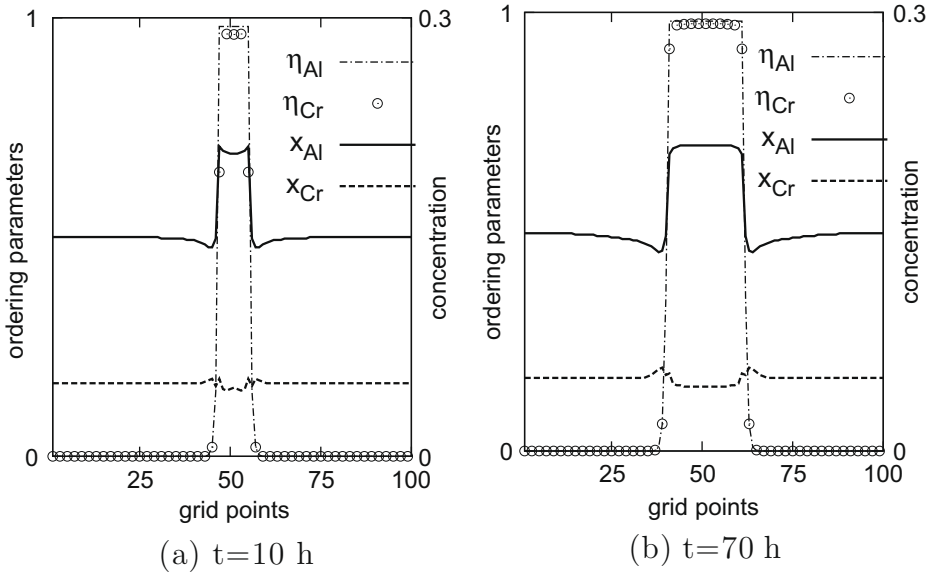

Fig. 4. Evolution of concentration and LRO parameter η^1 for Al and Cr in Ni–15Al–5Cr at.% alloy at two different stages of the growth of a precipitate. The equilibrium concentrations of the precipitate are $X^{eq}_{Al} = 0.18$ and $X^{eq}_{Cr} = 0.05$.

Simulation tests were extended to include multiple precipitate particles for more realistic growth and coarsening simulations. We used Poisson seeding [23] as a way of simulating starting microstructures. The nuclei were introduced into individual cells randomly. The order parameters for each of the nuclei were also assigned randomly to maintain roughly equal amounts of the four types of antiphase domains in the precipitates. The simulated evolution of alloy Ni–10Al–10Cr at.% exhibits the typical steady nucleation/growth regime followed by a coarsening regime, where the precipitate area fraction approaches its equilibrium value. The ordering profiles for Al and Cr are shown separately in Fig. 5 at two different stages of the evolution, where the four types of ordered domain structures having different combinations of the three LRO parameters (as discussed in Section 2.1.2) are represented with four different colors (red, blue, white, aquamarine) and the disordered matrix phase is in black. The profiles of the ordered domains for the two solute elements overlap each other during the entire evolution as shown in the representative snapshots in Fig. 5. These proof-of-principle tests demonstrate that the model can accurately describe the compositional and structural changes associated with the precipitation and evolution of the γ' phase.

It has long been recognized that the ternary diffusion behavior is quite different from that of the binary systems. A classic example to demonstrate this difference is the so-called uphill diffusion, which represents a situation where the diffusing substance can diffuse toward a higher concentration region. The uphill diffusion is widely observed in system of more than two components since the classic Darken experiment in steels [24]. In binary systems, the diffusion is driven by the concentration gradient. The species diffuse toward a region of lower concentration and therefore uphill diffusion is not expected.

In ternary or higher-order systems, the driving force for diffusion is attributed to the negative gradient of the chemical potential of the diffusing substance [24]. While the concentration gradient of the diffusing substance certainly contributes to the gradient of the chemical potential, the presence of other alloying components could alter its chemical potential as well. As a result, the diffusion path of a species in a ternary or higher-order systems is dependent on the concentration gradients of all the constituent components.

To examine the capability of the phase-field method in capturing the essential physics of ternary diffusion, we choose a few diffusion couples to simulate the evolution of concentration profiles under isothermal heat treatment. The following three types of diffusion couples are studied (at.%):

(1) Ni–15Al–1Cr/Ni–15Al–5Cr.
(2) Ni–15.5Al–1Cr/Ni–15Al–5Cr.
(3) Ni–18Al–1Cr/Ni–15Al–5Cr.

In all these diffusion couples, the right end of the alloys are the same, i.e. Ni–15Al–5Cr. The Cr content are held constant (1 at.%) for the alloys on the left end while the Al concentration varies. In couple 1, the Al content is 15 at.%, i.e. the same as in the alloy on the right end. Therefore there exists only a gradient in Cr concentration but not in Al across the couple interface. A slight increase in Al concentration is introduced in couple 2 leading to an opposite sign in the concentration gradient of Al and Cr across the couple. In couple 3, the concentration of Al is further increased leading to a higher concentration gradient in Al across the couple. At the beginning of the simulation, two long slabs (each represented by a 200×50 uniform mesh) of alloys are "welded" together to form a

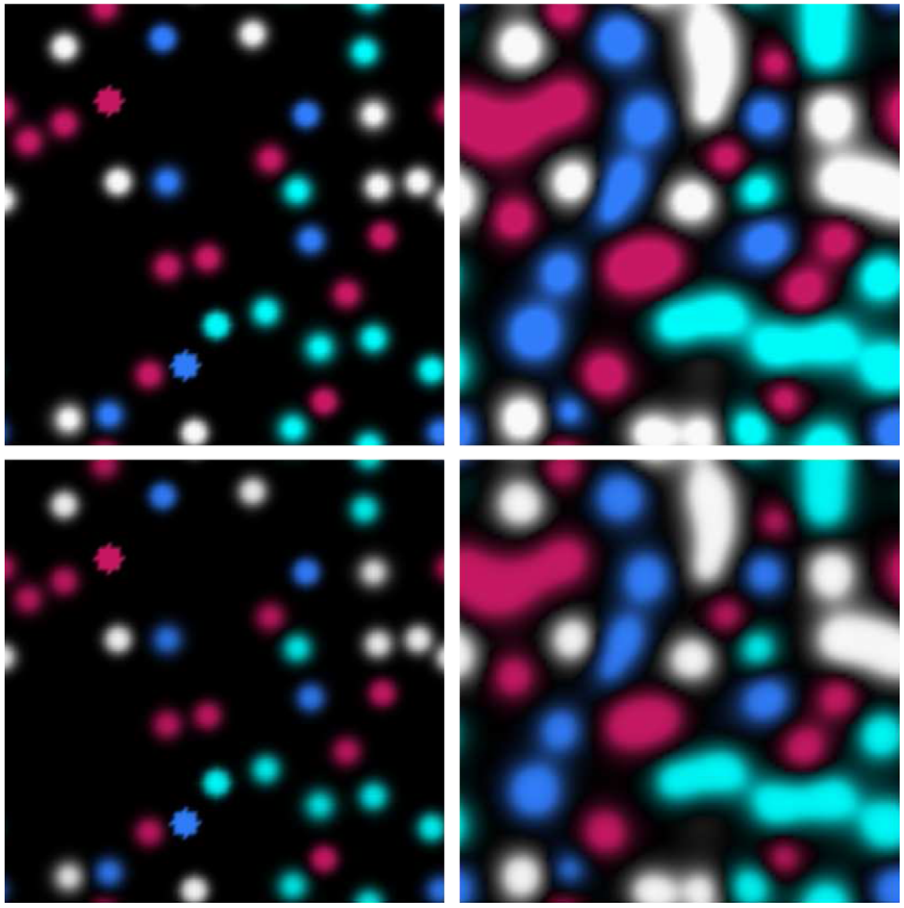

Fig. 5. Snapshots of the ordering domains at $t = 10$, 150 (h) (left to right) during the γ' precipitation from the γ matrix in Ni–10Al–10Cr at.% alloy. Top row shows the ordering profiles of Al and the bottom Cr.

400×50 mesh for the simulation under isothermal holding. The alloys on both ends of the couples are homogeneous in concentration and have a single phase of γ for the sake of simplicity. It was assumed that nucleation was negligible in these regimes and that mixing was dominated by diffusion. Therefore, no nucleation was utilized in the simulation.

Fig. 6 shows a snapshot of the concentration of Al (the faster diffusing species relative to Cr in Ni–Al–Cr systems) as a function of the distance from the original interface after isothermal annealing at 873 K. The positive (negative) sign of the distance indicates the right (left) hand side of couple. The concentration shown is an average value of all grid points at a given distance from the interface. Only the diffusion zone (central portion of the simulation cell) is shown. It is interesting to observe uphill diffusion in couple 1 despite the absence of a Al concentration gradient. Similar uphill diffusion has been observed recently for Ru diffusion in a Ni–Re–Ru diffusion couple (Ni–10Re–10Ru/Ni–10Ru) experiment [25]. They related this uphill diffusion of Ru to the negative cross-term of the diffusion coefficient ($D^{\mathrm{Ni}}_{\mathrm{RuRe}}$), which promoted the more mobile Ru atoms to diffuse to the Re rich side of the interface [25]. We will examine this factor later. In couple 2, the Al concentration on the left side alloy is slightly higher. If this is a binary system without Cr presence on both ends of the couple, one would expect the Al concentration goes lower across the couple from the left to the right. In the current situation

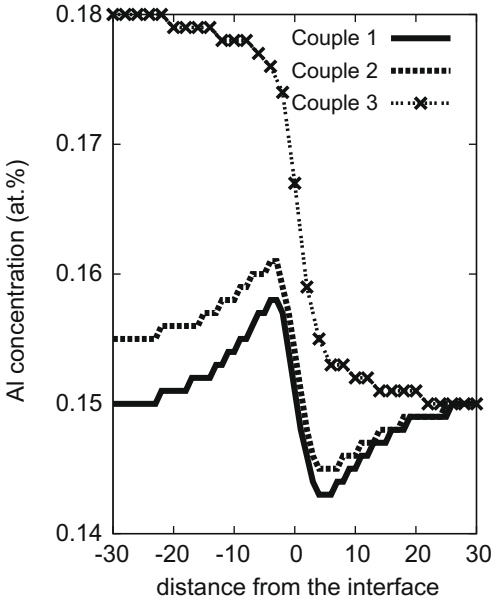

Fig. 6. Concentration profile of Al in three diffusion couples.

with the presence of Cr on both ends, we observe the uphill diffusion instead. With the Al concentration further increases for the alloy on the left end in couple 3, the gradient of Al is further increased across the couple. This increase in the Al concentration gradient is enough to overcome the effect of Cr concentration gradient on the chemical potential imbalance across the couple leading to the normal diffusion of Al across the couple interface.

Fig. 7 presents the chemical potential profiles across the interface for Al and Cr for the three couples. As can be seen for couple 1 in Fig. 7a, the chemical potential of Al exhibits a positive correlation with the Cr content. With lower Cr concentration on the left, chemical potential is lower on the left half and higher on the right, leading to the uphill diffusion. While the Al chemical potential gradient decreases in couple 2 due to higher concentration of Al on the left side of the couple, the alloy on the left still has a lower chemical potential for Al. As the Al concentration is further increased to 18.0 at.% for the alloy on the left side in couple 3, which represents a 3% difference in Al concentration across the interface of the couple, the sign of the Al chemical potential gradient is changed as compared to those in couples 1 and 2. This shows that a 3% difference in Al concentration has overcome the effect of a 4% Cr concentration difference across the couple. As such, the uphill diffusion is not observed in diffusion couple 3. As for the chemical potential of Cr (Fig. 7b), the increase in Al concentration on the left has decreased its gradient across the interface (compare the three couples), but the 4% difference in Cr concentration on both ends is significant and therefore the chemical potential is always lower on the left side with a lower Cr concentration.

We now examine the effect of the diffusion coefficients. According to the Fick–Onsager law [26,27], the one-dimensional (1-D) diffusion of Al in the ternary diffusion couple can be described as:

$$\frac{\partial x_{\mathrm{Al}}}{\partial t}=\frac{\partial}{\partial x}\left(D_{\mathrm{AlAl}}\frac{\partial x_{\mathrm{Al}}}{\partial x}\right)+\frac{\partial}{\partial x}\left(D_{\mathrm{AlCr}}\frac{\partial x_{\mathrm{Cr}}}{\partial x}\right) \tag{28}$$

where D_{AlAl} is the interdiffusion coefficient describing the influence of Al concentration gradient on its own fluxes, and D_{AlCr} the cross-term of the interdiffusion coefficients reflecting the influence of the concentration gradient of Cr on the flux of Al. In our phase-field formulation, the diffusion mobilities are used to play the role of the diffusion coefficients as shown below the 1-D version of the diffusion equation for Al from Eq. (11):

$$\frac{\partial x_{\mathrm{Al}}}{\partial t}=V_m^2\left[\frac{\partial}{\partial x}\left(M_{\mathrm{AlAl}}\frac{\partial(\delta F/\delta x_{\mathrm{Al}})}{\partial x}\right)+\frac{\partial}{\partial x}\left(M_{\mathrm{AlCr}}\frac{\partial(\delta F/\delta x_{\mathrm{Cr}})}{\partial x}\right)\right] \tag{29}$$

where $\delta F/\delta x_{\mathrm{Al}}$ and $\delta F/\delta x_{\mathrm{Cr}}$ are the chemical potentials for Al and Cr, respectively. Similar to the interdiffusion coefficients, M_{AlAl} is the diffusion mobility that characterizes the influence of Al chemical potential gradient on its own fluxes, M_{AlCr} the cross-term of the diffusion mobility that describes the influence of Cr chemical potential gradient on the flux of Al.

Fig. 8 shows the profiles of three diffusion mobility terms, i.e. $M_{\mathrm{AlAl}}, M_{\mathrm{AlCr}}$ and M_{CrCr}, across the interface for couple 1. As can be seen from the plot, the value of M_{AlAl} is about an order of magnitude larger than that of M_{CrCr}, confirming that Al is the faster diffuser. The cross-term of the diffusion mobility M_{AlCr} is negative and its value is more than an order of magnitude smaller than that of M_{AlAl}. The negative sign means that the Cr chemical potential gradient (mainly controlled by the Cr concentration gradient) in couple 1 would promote Al to diffuse from

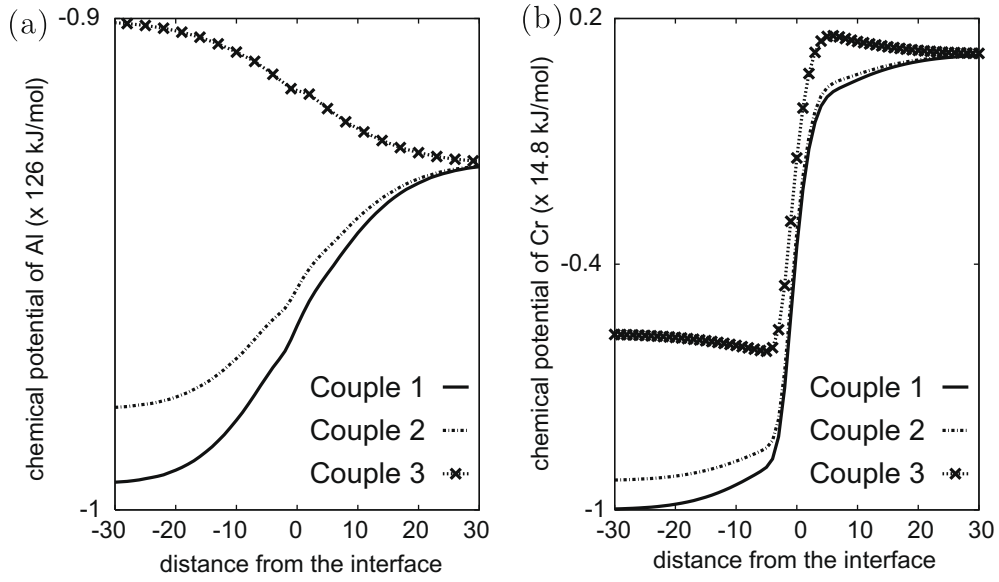

Fig. 7. Chemical potentials of Al (a) and Cr (b) for the three couples with the concentration profile shown in Fig. 6. Note that the scales in the two figures are different.

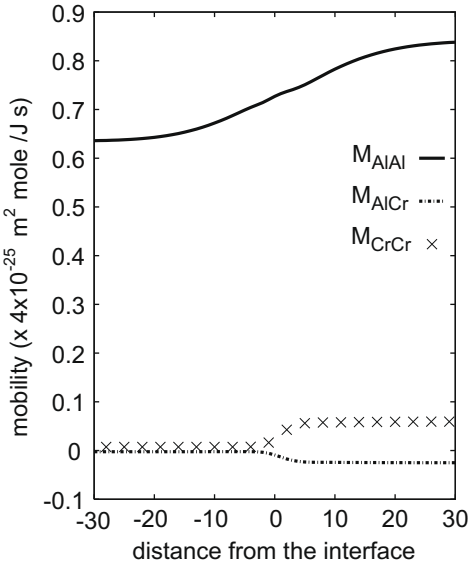

Fig. 8. Profiles of diffusion mobilities for couple 1 corresponding to the concentration profile shown in Fig. 6.

the left to the right side due to a negative Cr concentration gradient across the interface. Therefore, this cross-diffusion is not responsible for the uphill diffusion observed in couple 1. In addition, the relatively small value of M_{AlCr} makes the direct contribution of the Cr concentration gradient to Al diffusion far less significant than that of its effect on the chemical potential gradient across the interface.

Here we discuss briefly some potential applications of this model. We have demonstrated that the model can accurately describe the precipitation of γ' in the γ matrix of Ni-based superalloys. This model can be applied to study quantitatively the precipitation behavior in the Ni–Al–Cr system. For example, by examining the evolution of the concentrations in the precipitate under well-designed simulation conditions, such as various initial concentration/ordering profiles for the nucleus or precipitate, may provide some insight to the so-called Cr-trapping behavior observed experimentally [28], a situation where the concentration of Cr in the precipitate decreases monotonically with the growth of the precipitate, while the CALPHAD approach predicts the opposite trend. Details will be published in a forthcoming paper. This model can also serve as the basis for a pseudo-ternary model that can simulate precipitation behavior in Ni-based superalloys. Also we treated explicitly the misfit effect due to partitioning of Al and Cr in our elastic energy formulation. In this work, we set the misfit to zero since no significant misfit is reported for Ni–Al–Cr systems. However, this formulation is general and could be useful for studying the effect of misfit arising from multiple sources for alloy design purposes. We studied the uphill diffusion without involving γ' microstructure. However, it is straightforward to incorporate a dynamically evolving γ and γ' microstructures on both sides of the diffusion couple and study how different microstructure characteristics (e.g. phase fraction and their size distribution) affect the diffusion path [29]. Considering that we have implemented the most up-to-date mobility database, the accuracy of diffusion path prediction might be improved.

4. Conclusions

A ternary phase-field model based on the Ni–Al–Cr system was developed. The model is linked directly to commercial CALPHAD software and implements a diffusion mobility database that recently became available, and includes the contribution from the ordered phase. The direct linkage with commercial CALPHAD software provides quantitative thermodynamic driving forces. In addition, a more accurate description of the diffusion behavior is achieved in the alloy system by including contribution from the ordered state. Simulations show that the model can qualitatively represent the compositional and structural changes associated with the $\gamma \rightarrow \gamma'$ transformation in the Ni-based superalloys. Uphill diffusion of Al is observed in a few diffusion couples showing the significant influence of Cr on the chemical potential of Al.

This model can be applied to study quantitatively precipitation behavior in the Ni–Al–Cr system. This model can also serve as the basis for a pseudo-ternary model that can simulate precipitation behavior in Ni-based superalloys, including the misfit effect due to partitioning of Al and Cr using the elastic energy formulation. Given the most up-to-date mobility database that is incorporated in the model, this model might be employed to study the microstructure effect on diffusion pathways with higher accuracy.

Acknowledgements

We appreciate the helpful discussions with Chris Woodward and Dennis Dimiduk at AFRL. Y.H.W. is grateful that Dr. Campbell from NIST made the diffusion database available before publication and for her helpful discussions. Computations were performed at the AFRL/MSRC high performance computing center. Y.H.W. acknowledges support from the Air Force Research Laboratory (AFRL) through Contracts #FA8650-04-D-5233 and FA8650-04-D-5235 with UES Inc. JVL acknowledges support from the PET program under the DoD High Performance Computing Modernization Program.

References

[1] Wang Y, Banerjee D, Su C, Khachaturyan A. Acta Mater 1998;46:2983.
[2] Rubin G, Khachaturyan A. Acta Mater 1999;47:1995.
[3] Zhu J, Liu Z, Vaithyanathan V, Chen L. Scr Mater 2002;46:401.
[4] Zhu J, Wang T, Ardell A, Zhou S, Liu Z, Chen L. Acta Mater 2004;52:2837.
[5] Wen Y, Simmons J, Shen C, Woodward C, Wang Y. Acta Metall 2003;51:1123.
[6] Wen Y, Wang B, Simmons J, Wang Y. Acta Metall 2006;54:2087.
[7] Grafe U, Bottger B, Tiaden J, Fries S. Scr Mater 2000;42:1179.
[8] Cha P, Yeon D, Yoon J. Acta Mater 2001;49:3295.
[9] Yeon D, Cha P, Yoon J. Scr Mater 2001;45:661.

[10] Wu K, Chang Y, Wang Y. Scr Mater 2004;50:1145.
[11] Huang W, Chang Y. Intermetallics 1999;7:863.
[12] Merchant S, Notis M. Mater Sci Eng 1984;66:47.
[13] N. Saunders, in: Superalloys, TMS, 1996, p. 101.
[14] Dupin N, Ansara I, Sundman B. Calphad 2001;25:279.
[15] Engstrom A, Agren J. Z Metallkd 1996;87:92.
[16] Campbell C. Acta Mater 2008;56:4277.
[17] Hillert M, Staffansson L-I. Acta Chem Scand 1970;24:3618.
[18] Sundman B, Agren J. J Phys Chem Solids 1981;42:297.
[19] Ansara I, Dupin N, Lukas H, Sundman B. J Alloy Compd 1997;247:20.
[20] Chen L. Annu Rev Mater Res 2002;32:113.
[21] Cahn JW, Hilliard JE. J Chem Phys 1958;28:258.
[22] Andersson J, Agren J. J Appl Phys 1992;72:1350.
[23] Simmons J, Shen C, Wang Y. Scr Mater 2000;43:935.
[24] Darken L. Trans AIME 1949;180:430.
[25] Hobbs R, Karunaratne M, Tin S, Reed R, Rae C. Mater Sci Eng A 2007;460–461:587.
[26] Fick A. Annalen Physik Chemie 1855;94:59.
[27] Onsager L. Ann NY Adad Sci 1945;46:241.
[28] Sudbrack C, Noebe R, Seidman D. Acta Mater 2006;54:3199.
[29] Wu K, Morral J, Wang Y. Acta Mater 2001;49:3401.